Modeling Lossy Anisotropic Dielectric Waveguides with the Method of Lines

Pierre Berini, *Member, IEEE*, and Ke Wu, *Senior Member, IEEE*

Abstract— **This paper presents a new formulation useful for modeling waveguides constructed from lossy inhomogeneous anisotropic media. Our approach is based on a pair of Sturm–Liouville type wave equations that have been derived to handle inhomogeneous, diagonalized complex permittivity and permeability tensors. The method of lines is then applied to these wave equations, and related field equations, creating an indirect eigenvalue problem that correctly models this class of structure. Some refinements to the method of lines are also proposed, particularly, regarding the construction of the modal matrices found in the eigenvalue problem. Using our approach, modal dispersion curves have been computed for millimeter-wave and optical structures. Comparisons made with results available from the literature validate our approach.**

I. Introduction

DIELECTRIC waveguides are used almost exclusively for the transmission of electromagnetic energy at optical frequencies. They are also well suited to waveguiding at millimeter-wave frequencies since compact low loss structures can be constructed. Dielectric guides, however, must be accurately modeled if a circuit design is to be functional in the end. This is particularly true in integrated optics where the guides are often constructed on complex multilayer structures and where a precise knowledge of propagation constants is desirable. Rigorous and efficient numerical techniques are therefore called upon to provide millimeter-wave and optical circuit designers with appropriate mathematical or physical models of such structures.

The most useful numerical techniques will function with limited computing resources while providing accurate solutions to a wide range of waveguiding problems. Additionally, a method should be general enough to model important material properties such as losses, inhomogeneity, and anisotropy. Some vectorial methods, such as the finite element [1]–[3] and finite difference [4] methods have been used to analyze lossy inhomogeneous anisotropic waveguides. We have chosen to work with the method of lines (MoL) since it is also a rigorous vectorial technique. Furthermore, it is well known for its numerical performance; that is, its accuracy, speed of computation, and minimal memory requirements.

The application of the MoL to the resolution of wave equations that generate the mode spectrum of isotropic dielectric waveguides is well documented. Work described by Diestel [5], [6], Pregla *et al.* [7]–[9] are most notable here. Losses are easily introduced into this formulation as shown in [10] and [11] where metal strips having a finite thickness are modeled as lossy inhomogeneous dielectrics. Some efforts to include material anisotropy have been reported where homogeneous anisotropic substrates were used to support strip-line waveguides [12], [13]. Some work has also been done regarding homogeneous gyroelectric and gyromagnetic materials [7], [14].

In this paper, we are concerned with the application of the MoL approach to solve the wave and field equations that govern guiding in structures constructed from lossless or lossy materials that are both inhomogeneous and anisotropic. To our knowledge, present formulations applying the MoL cannot handle this situation which is of practical importance, especially in integrated optics. The wave and field equations to be solved are derived in Section II followed by a description of the indirect eigenvalue problem obtained by applying the MoL. Numerical results and a discussion are given in Section III.

II. Formulation

In this section, the wave and field equations that must be solved are derived directly from Maxwell's equations. The method of lines is then applied to these equations such that an appropriate indirect eigenvalue problem is created. Alternative formulations for the modal matrices are proposed.

A. Wave and Field Equations

Maxwell's equations are written in the frequency domain for source-free anisotropic inhomogeneous media

$$\nabla \times \boldsymbol{H} = j\omega\bar{\epsilon} \cdot \boldsymbol{E} \tag{1}$$

$$\nabla \times \boldsymbol{E} = -j\omega\bar{\mu} \cdot \boldsymbol{H} \tag{2}$$

$$\nabla \cdot (\bar{\epsilon} \cdot \boldsymbol{E}) = 0 \tag{3}$$

$$\nabla \cdot (\bar{\mu} \cdot \boldsymbol{H}) = 0 \tag{4}$$

where $\bar{\epsilon}$ and $\bar{\mu}$ are diagonal second rank tensors sharing common principal axes. We expand these tensors in a cartesian

Manuscript received September 1, 1995; revised January 17, 1996. This work was supported grants from NSERC and FCAR.

P. Berini was with the Centre de Recherches Poly-GRAMES, Département de génie électrique et informatique, École Polytechnique de Montréal. He is now with the Department of Electrical Engineering, University of Ottawa, Ottawa, Ontario K1N 6N5 Canada.

K. Wu is with the Centre de Recherches Poly-GRAMES, Département de génie électrique et informatique, École Polytechnique de Montréal, Succursale Centre-Ville, Montréal, Québec H3C 3A7 Canada.

Publisher Item Identifier S 0018-9480(96)03028-1.

coordinate system and write in matrix notation

$$\overline{\epsilon} = \begin{bmatrix} \epsilon_{xx} & & \\ & \epsilon_{yy} & \\ & & \epsilon_{zz} \end{bmatrix} \tag{5}$$

and

$$\overline{\mu} = \begin{bmatrix} \mu_{xx} & & \\ & \mu_{yy} & \\ & & \mu_{zz} \end{bmatrix}. \tag{6}$$

For inhomogeneous waveguides constructed from linear materials, the components of the above tensors depend on x and y only $\epsilon_{ii}(x,y), \mu_{ii}(x,y)$; the direction of wave propagation is taken along the $+z$ axis. Both dielectric and ohmic losses are included since μ_{ii} and ϵ_{ii} are taken to be complex quantities defined as $\mu_{ii} = \mu'_{ii} - j\mu''_{ii}$ and $\epsilon_{ii} = \epsilon'_{ii} - j(\epsilon''_{ii} + \sigma_{ii}/\omega)$ where σ_{ii} are components of the conductivity tensor.

Maxwell's curl equations (1) and (2) are coupled first order differential equations. They become uncoupled by applying the following sequence of mathematical operations $\nabla \times \overline{\mu}^{-1} \cdot (2)$ into (1) and $\nabla \times \overline{\epsilon}^{-1} \cdot (1)$ into (2). Second order vectorial wave equations, which are rigorously equivalent to Maxwell's curl equations, are then obtained for $\boldsymbol{E}$ and $\boldsymbol{H}$

$$\nabla \times \overline{\mu}^{-1} \cdot \nabla \times \boldsymbol{E} - \omega^2 \overline{\epsilon} \cdot \boldsymbol{E} = 0 \tag{7}$$

$$\nabla \times \overline{\epsilon}^{-1} \cdot \nabla \times \boldsymbol{H} - \omega^2 \overline{\mu} \cdot \boldsymbol{H} = 0. \tag{8}$$

We may immediately remove the y dependence in $\overline{\epsilon}$ and $\overline{\mu}$ since in the MOL, the inhomogeneous part of the structure along y is divided into a number of homogeneous layers and boundary conditions are applied between them. The two vectorial wave equations (7) and (8) are then expanded into six scalar wave equations. In inhomogeneous anisotropic media, each scalar wave equation couples with at least an other making their solution difficult. However, if we consider TE^x ($E_x^{\mathrm{TE}} = 0$) and TM^x ($H_x^{\mathrm{TM}} = 0$) modes only and make use of (3) and (4) accordingly, we obtain some uncoupled scalar wave equations for both these families of modes. The superposition of the TE^x and TM^x modes will then completely characterize any mode propagating in the structure, including hybrid ones.

The TE^x modes are obtained by solving the following wave equation for the E_y field component:

$$\mu_{rx}\frac{\epsilon_{zz}}{\epsilon_{yy}}\frac{\partial}{\partial x}\left[\frac{1}{\mu_{zz}}\frac{\partial}{\partial x}E_y^{\mathrm{TE}}\right] + \frac{\partial^2}{\partial y^2}E_y^{\mathrm{TE}} + \left(\frac{\epsilon_{zz}}{\epsilon_{yy}}\gamma^2 + \omega^2\mu_{xx}\epsilon_{zz}\right)E_y^{\mathrm{TE}} = 0 \tag{9}$$

and similarly, the TM^x modes are obtained by solving the following wave equation for the H_y field component:

$$\epsilon_{xx}\frac{\mu_{zz}}{\mu_{yy}}\frac{\partial}{\partial x}\left[\frac{1}{\epsilon_{zz}}\frac{\partial}{\partial x}H_y^{\mathrm{TM}}\right] + \frac{\partial^2}{\partial y^2}H_y^{\mathrm{TM}} + \left(\frac{\mu_{zz}}{\mu_{yy}}\gamma^2 + \omega^2\mu_{zz}\epsilon_{xx}\right)H_y^{\mathrm{TM}} = 0 \tag{10}$$

where we have defined the complex propagation constant γ such that $\partial/\partial z = -\gamma$ and $\gamma = \alpha + j\beta$. The above wave equations are Sturm–Liouville type differential equations written in self-adjoint form. They simplify to Helmhotlz equations when we no longer have an x dependence in $\overline{\epsilon}$ and $\overline{\mu}$.

The x and z oriented electric and magnetic field components of the modes propagating in the structure are related to the TE^x and TM^x modes via the following equations:

$$E_x = \frac{-1}{j\omega\gamma}\left[\frac{\partial}{\partial x}\left(\frac{1}{\epsilon_{zz}}\frac{\partial}{\partial x}H_y^{\mathrm{TM}}\right) + \omega^2\mu_{yy}H_y^{\mathrm{TM}}\right] \tag{11}$$

$$E_z = \frac{1}{\gamma}\frac{\epsilon_{yy}}{\epsilon_{zz}}\frac{\partial}{\partial y}E_y^{\mathrm{TE}} + \frac{1}{j\omega\epsilon_{zz}}\frac{\partial}{\partial x}H_y^{\mathrm{TM}} \tag{12}$$

$$H_x = \frac{1}{j\omega\gamma}\left[\frac{\partial}{\partial x}\left(\frac{1}{\mu_{zz}}\frac{\partial}{\partial x}E_y^{\mathrm{TE}}\right) + \omega^2\epsilon_{yy}E_y^{\mathrm{TE}}\right] \tag{13}$$

$$H_z = \frac{-1}{j\omega\mu_{zz}}\frac{\partial}{\partial x}E_y^{\mathrm{TE}} + \frac{1}{\gamma}\frac{\mu_{yy}}{\mu_{zz}}\frac{\partial}{\partial y}H_y^{\mathrm{TM}}. \tag{14}$$

The Sturm–Liouville wave equations (9) and (10), along with the above field equations (11)–(14), are solved for the propagation constant γ using appropriate boundary conditions applied at the horizontal and vertical limits.

B. Application of the Method of Lines

A thorough description of the MoL technique along with some results are given in [7] and references therein. However, since we are solving a different set of differential equations, we include for clarity of presentation and completeness, some intermediate steps and give details in the Appendix.

In the MoL, the differential equations to be solved are discretized along one dimension only for a two-dimensional (2-D) problem. The equations are then solved analytically in the remaining dimension while applying boundary conditions between consecutive layers. A large number of lines can thus be used to discretise one dimension while an arbitrary large number of layers can be used to describe the inhomogeneous character of the structure along the other dimension. The required computing resources are modest and the numerical accuracy of the approach we are using is of order h^2; h being the discretization interval. Furthermore, for a lossless structure, β exhibits a monotonic variation with h thus making possible numerical extrapolation to higher precision values.

Fig. 1 illustrates an arbitrary waveguide structure composed of a sequence of layers that are homogeneous or inhomogeneous along x. Also shown are the shifted E and H line systems where, respectively, the E_y^{TE} and H_y^{TM} field components are solved. The nonequidistant discretization scheme is shown for the case of electric wall lateral boundary conditions.

We approximate the differential operators along x using nonequidistant finite difference techniques as detailed in [15] and [7]. The required discretized differential operators are listed below in matrix form where the top notation refers to electric-electric or electric-magnetic lateral wall combinations (ew-ew, ew-mw) and the bottom notation refers to the magnetic-magnetic or magnetic-electric lateral wall (mw-mw,

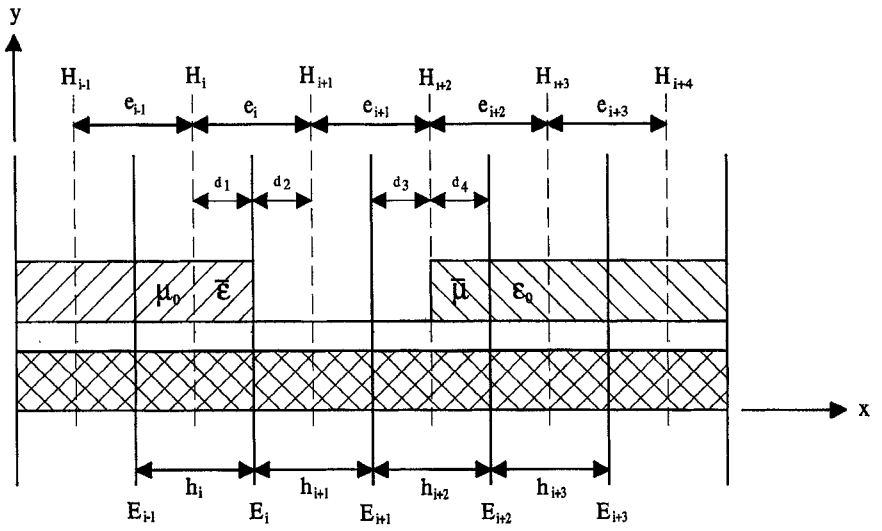

Fig. 1. Waveguide structure discretized by two shifted line systems E and H for electric wall lateral boundary conditions.

mw-ew) combinations

$$\frac{\partial}{\partial x}\boldsymbol{E}_{\boldsymbol{y}}^{n,\mathrm{TE}} = \begin{Bmatrix} \frac{1}{h}D_x & = \frac{1}{h}r_h D r_e \\ -\frac{1}{h}D_x^t & = -\frac{1}{h}r_h D^t r_e \end{Bmatrix} \boldsymbol{E}_{\boldsymbol{y}}^{n,\mathrm{TE}} \tag{15}$$

$$\frac{\partial}{\partial x}\boldsymbol{H}_{\boldsymbol{y}}^{n,\mathrm{TM}} = \begin{Bmatrix} -\frac{1}{h}D_x^t & = -\frac{1}{h}r_e D^t r_h \\ \frac{1}{h}D_x & = \frac{1}{h}r_e D r_h \end{Bmatrix} \boldsymbol{H}_{\boldsymbol{y}}^{n,\mathrm{TM}} \tag{16}$$

$$\frac{\partial^2}{\partial x^2}\boldsymbol{E}_{\boldsymbol{y}}^{n,\mathrm{TE}} = -\frac{1}{h^2}P_e = \begin{Bmatrix} -\frac{1}{h^2}D_x^t D_x \\ -\frac{1}{h^2}D_x D_x^t \end{Bmatrix} \boldsymbol{E}_{\boldsymbol{y}}^{n,\mathrm{TE}} \tag{17}$$

$$\frac{\partial^2}{\partial x^2}\boldsymbol{H}_{\boldsymbol{y}}^{n,\mathrm{TM}} = -\frac{1}{h^2}P_h = \begin{Bmatrix} -\frac{1}{h^2}D_x D_x^t \\ -\frac{1}{h^2}D_x^t D_x \end{Bmatrix} \boldsymbol{H}_{\boldsymbol{y}}^{n,\mathrm{TM}} \tag{18}$$

$$\frac{\partial}{\partial x}\left(\mu_{zz}^{-1}\frac{\partial}{\partial x}\boldsymbol{E}_{\boldsymbol{y}}^{n,\mathrm{TE}}\right) = -\frac{1}{h^2}Psl_e = \begin{Bmatrix} -\frac{1}{h^2}D_x^t[\mu_{zz}]_h^{-1}D_x \\ -\frac{1}{h^2}D_x[\mu_{zz}]_h^{-1}D_x^t \end{Bmatrix} \boldsymbol{E}_{\boldsymbol{y}}^{n,\mathrm{TE}} \tag{19}$$

$$\frac{\partial}{\partial x}\left(\epsilon_{zz}^{-1}\frac{\partial}{\partial x}\boldsymbol{H}_{\boldsymbol{y}}^{n,\mathrm{TM}}\right) = -\frac{1}{h^2}Psl_h = \begin{Bmatrix} -\frac{1}{h^2}D_x[\epsilon_{zz}]_e^{-1}D_x^t \\ -\frac{1}{h^2}D_x^t[\epsilon_{zz}]_e^{-1}D_x \end{Bmatrix} \boldsymbol{H}_{\boldsymbol{y}}^{n,\mathrm{TM}}. \tag{20}$$

Matrix D is as given in [7]; although the same notation is used, it must be noted that the first-order finite difference operator D_x is different for all combinations of lateral walls. We have included the second order operators $P_{e,h}$ as they are useful for treating homogeneous layers, usually present in composite structures. The normalized fields $\boldsymbol{E}_{\boldsymbol{y}}^{n,\mathrm{TE}}$ and $\boldsymbol{H}_{\boldsymbol{y}}^{n,\mathrm{TM}}$ are defined such that the second-order finite difference operators $P_{e,h}$ and $Psl_{e,h}$ are real symmetric matrices when a nonequidistant discretization scheme is used. The normalized quantities relate to the discretized fields via the following matrix relations:

$$\begin{aligned} \boldsymbol{E}_{\boldsymbol{y}}^{\mathrm{TE}} &= r_e \boldsymbol{E}_{\boldsymbol{y}}^{n,\mathrm{TE}} \\ \frac{\partial}{\partial x}\boldsymbol{E}_{\boldsymbol{y}}^{\mathrm{TE}} &= r_h \frac{\partial}{\partial x}\boldsymbol{E}_{\boldsymbol{y}}^{n,\mathrm{TE}} \\ \frac{\partial^2}{\partial x^2}\boldsymbol{E}_{\boldsymbol{y}}^{\mathrm{TE}} &= r_e \frac{\partial^2}{\partial x^2}\boldsymbol{E}_{\boldsymbol{y}}^{n,\mathrm{TE}} \end{aligned} \tag{21}$$

and

$$\begin{aligned} \boldsymbol{H}_{\boldsymbol{y}}^{\mathrm{TM}} &= r_h \boldsymbol{H}_{\boldsymbol{y}}^{n,\mathrm{TM}} \\ \frac{\partial}{\partial x}\boldsymbol{H}_{\boldsymbol{y}}^{\mathrm{TM}} &= r_e \frac{\partial}{\partial x}\boldsymbol{H}_{\boldsymbol{y}}^{n,\mathrm{TM}} \\ \frac{\partial^2}{\partial x^2}\boldsymbol{H}_{\boldsymbol{y}}^{\mathrm{TM}} &= r_h \frac{\partial^2}{\partial x^2}\boldsymbol{H}_{\boldsymbol{y}}^{n,\mathrm{TM}} \end{aligned} \tag{22}$$

where the normalization matrices r_e and r_h are written

$$r_e = \left[\sqrt{\frac{h}{e_i}}\right]_{\mathrm{diag}} \qquad r_h = \left[\sqrt{\frac{h}{h_i}}\right]_{\mathrm{diag}} \tag{23}$$

and h is taken as the minimal discretization distance.

Our wave equations, (9) and (10), are discretized within each layer of our composite structure by introducing the second-order finite difference operators defined above

$$\left(-\frac{1}{h^2}[\mu_{xx}]_e[\epsilon_{zz}]_e[\epsilon_{yy}]_e^{-1}Psl_e + \omega^2[\mu_{xx}]_e[\epsilon_{zz}]_e + \gamma^2[\epsilon_{zz}]_e[\epsilon_{yy}]_e^{-1}\right)\boldsymbol{E}_{\boldsymbol{y}}^{n,\mathrm{TE}} + \frac{\partial^2}{\partial_y^2}\boldsymbol{E}_{\boldsymbol{y}}^{n,\mathrm{TE}} = 0 \tag{24}$$

$$\left(-\frac{1}{h^2}[\epsilon_{xx}]_h[\mu_{zz}]_h[\mu_{yy}]_h^{-1}Psl_h + \omega^2[\mu_{zz}]_h[\epsilon_{xx}]_h + \gamma^2[\mu_{zz}]_h[\mu_{yy}]_h^{-1}\right)\boldsymbol{H}_{\boldsymbol{y}}^{n,\mathrm{TM}} + \frac{\partial^2}{\partial_y^2}\boldsymbol{H}_{\boldsymbol{y}}^{n,\mathrm{TM}} = 0. \tag{25}$$

The diagonal matrices $[\epsilon_{xx}]_h$, $[\mu_{yy}]_h$ and $[\mu_{zz}]_h$ are created from the functions $\epsilon_{xx}(x), \mu_{yy}(x)$ and $\mu_{zz}(x)$ sampled on the H lines while $[\mu_{xx}]_e, [\epsilon_{yy}]_e$ and $[\epsilon_{zz}]_e$ are formed from the functions $\mu_{xx}(x), \epsilon_{yy}(x)$ and $\epsilon_{zz}(x)$ sampled on the E lines.

Discontinuities in permittivity are rigorously accounted for if they are placed on an E line, where the tangential electric fields $E_{y,z}$ are continuous. The values of ϵ_{yy} and ϵ_{zz} on this line are found to be

$$\epsilon_{yy} = \frac{\epsilon_{yy,1} d_1 + \epsilon_{yy,2} d_2}{d_1 + d_2} \tag{26}$$

$$\epsilon_{zz} = \frac{\epsilon_{zz,1} d_1 + \epsilon_{zz,2} d_2}{d_1 + d_2} \tag{27}$$

Similarly we place discontinuities in permeability on an H line, where the tangential magnetic fields $H_{y,z}$ are continuous. The values of μ_{yy} and μ_{zz} on this line are

$$\mu_{yy} = \frac{\mu_{yy,3} d_3 + \mu_{yy,4} d_4}{d_3 + d_4} \tag{28}$$

$$\mu_{zz} = \frac{\mu_{zz,3} d_3 + \mu_{zz,4} d_4}{d_3 + d_4} \tag{29}$$

where the distances d_i, defined in Fig. 1, are required if the discretization is nonequidistant in the region of the discontinuities. The permittivities and permeabilities having subscripts i refer to the value of these quantities on either side of a discontinuity.

We now introduce the following transformations

$$\begin{aligned} \boldsymbol{E}_{\boldsymbol{y}}^{n,\mathrm{TE}} &= U_e \boldsymbol{\Phi}_{\boldsymbol{y}}^{\mathrm{TE}} \\ \boldsymbol{H}_{\boldsymbol{y}}^{n,\mathrm{TM}} &= U_h \boldsymbol{\Phi}_{\boldsymbol{y}}^{\mathrm{TM}} \end{aligned} \tag{30}$$

where U_e and U_h are nonsingular matrices. These transformations are substituted into our discretized wave equations which are then multiplied by U_e^{-1} and U_h^{-1}, respectively, as shown in (31) and (32) at the bottom of the page. The matrices U_e and U_h are selected such that the wave equations are diagonalized. This is achieved by eigenvalue decomposition where the matrices $U_{e,h}$ and $[\gamma_{e,h}^2]_{\mathrm{diag}}$ represent the eigenmatrices and eigenvalues respectively of the discretized wave equations.

Some observations can be made regarding the eigenvalue problem defined by (31); similar observations apply to (32). Most importantly, we note that for an inhomogeneous anisotropic layer, γ cannot be factored out of the transformation. This implies that the matrices U_e and $[\gamma_e^2]_{\mathrm{diag}}$, which are layer specific, must be recomputed whenever γ changes. We also point out that if the structure is lossless and we wish to model purely propagating or purely evanescent modes then the tri-diagonal matrix to be diagonalized becomes real and sign-symetric having real eigenvalues and eigenvectors only.

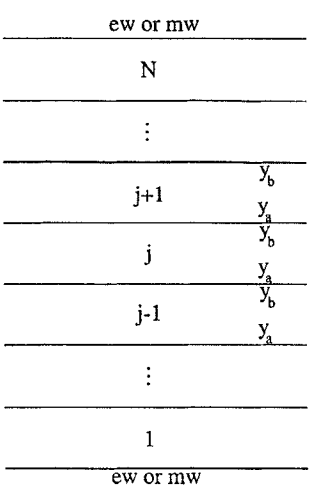

Fig. 2. Multilayer structure having arbitrary top and bottom boundary conditions.

If a layer is homogeneous, then our transformation matrices $U_{e,h}$ become identical to the orthonormal matrices $T_{e,h}$ found in [7] which are defined such that the second order finite difference operators $P_{e,h}$ are diagonalized $T_{e,h}^t P_{e,h} T_{e,h} = [\lambda_{e,h}^2]_{\mathrm{diag}}$ where $T_{e,h}^t$ denotes the transpose of $T_{e,h}$.

Diagonalising our wave equations has the desirable effect of uncoupling the elements of $\boldsymbol{\Phi}_{\boldsymbol{y}}^{\mathrm{TE,TM}}$, thus yielding a vectorial version of the familiar telegraph's equation

$$\frac{\partial^2}{\partial y^2} \boldsymbol{\Phi}_{\boldsymbol{y}}^{\mathrm{TE,TM}} - [\gamma_{e,h}^2]_{\mathrm{diag}} \boldsymbol{\Phi}_{\boldsymbol{y}}^{\mathrm{TE,TM}} = 0. \tag{33}$$

For an arbitrary layer j of thickness $d = y_b - y_a$ as shown in Fig. 2, the above equation has the well-known solution

$$\begin{bmatrix} \boldsymbol{\Phi}_{\boldsymbol{y}}^{\mathrm{TE,TM}}|_{y_b} \\ \dfrac{\partial}{\partial y} \boldsymbol{\Phi}_{\boldsymbol{y}}^{\mathrm{TE,TM}}|_{y_b} \end{bmatrix} = \begin{bmatrix} [\cosh(\gamma_{e,h} d)] & [\gamma_{e,h}]^{-1} [\sinh(\gamma_{e,h} d)] \\ [\gamma_{e,h}][\sinh(\gamma_{e,h} d)] & [\cosh(\gamma_{e,h} d)] \end{bmatrix} \cdot \begin{bmatrix} \boldsymbol{\Phi}_{\boldsymbol{y}}^{\mathrm{TE,TM}}|_{y_a} \\ \dfrac{\partial}{\partial y} \boldsymbol{\Phi}_{\boldsymbol{y}}^{\mathrm{TE,TM}}|_{y_a} \end{bmatrix} \tag{34}$$

or written in a more convenient form

$$\begin{bmatrix} \dfrac{\partial}{\partial y} \boldsymbol{\Phi}_{\boldsymbol{y}}^{\mathrm{TE,TM}}|_{y_a} \\ \dfrac{\partial}{\partial y} \boldsymbol{\Phi}_{\boldsymbol{y}}^{\mathrm{TE,TM}}|_{y_b} \end{bmatrix} = [\gamma_{e,h}] \begin{bmatrix} -[\tanh(\gamma_{e,h} d)]^{-1} & [\sinh(\gamma_{e,h} d)]^{-1} \\ -[\sinh(\gamma_{e,h} d)]^{-1} & [\tanh(\gamma_{e,h} d)]^{-1} \end{bmatrix} \cdot \begin{bmatrix} \boldsymbol{\Phi}_{\boldsymbol{y}}^{\mathrm{TE,TM}}|_{y_a} \\ \boldsymbol{\Phi}_{\boldsymbol{y}}^{\mathrm{TE,TM}}|_{y_b} \end{bmatrix} \tag{35}$$

$$-\overbrace{\frac{1}{h^2} U_e^{-1} ([\mu_{xx}]_e [\epsilon_{zz}]_e [\epsilon_{yy}]_e^{-1} Psl_e - h^2 \omega^2 [\mu_{xx}]_e [\epsilon_{zz}]_e - h^2 \gamma^2 [\epsilon_{zz}]_e [\epsilon_{yy}]_e^{-1}) U_e}^{[\gamma_e^2]} \boldsymbol{\Phi}_{\boldsymbol{y}}^{\mathrm{TE}} + \frac{\partial^2}{\partial_y^2} \boldsymbol{\Phi}_{\boldsymbol{y}}^{\mathrm{TE}} = 0 \tag{31}$$

$$-\underbrace{\frac{1}{h^2} U_h^{-1} ([\epsilon_{xx}]_h [\mu_{zz}]_h [\mu_{yy}]_h^{-1} Psl_h - h^2 \omega^2 [\mu_{zz}]_h [\epsilon_{xx}]_h - h^2 \gamma^2 [\mu_{zz}]_h [\mu_{yy}]_h^{-1}) U_h}_{[\gamma_h^2]} \boldsymbol{\Phi}_{\boldsymbol{y}}^{\mathrm{TM}} + \frac{\partial^2}{\partial_y^2} \boldsymbol{\Phi}_{\boldsymbol{y}}^{\mathrm{TM}} = 0 \tag{32}$$

where y_b refers to the position just under the top interface and y_a to the position slightly above the bottom interface such that all quantities are within layer j. The submatrices $[\cosh(\gamma_{e,h}d)]$, $[\sinh(\gamma_{e,h}d)]$ and $[\tanh(\gamma_{e,h}d)]$ are diagonal.

The field components tangential to the layers, E_x, E_z, H_x and H_z, are discretized on the system of E and H lines. The following transformations, applied to these discretized fields, are introduced

$$\begin{aligned}\tilde{\boldsymbol{e}}_{\boldsymbol{x}} &= T_h^t r_h^{-1} \boldsymbol{E}_{\boldsymbol{x}} \\ \tilde{\boldsymbol{e}}_{\boldsymbol{z}} &= T_e^t r_e^{-1} \boldsymbol{E}_{\boldsymbol{z}} \\ \tilde{\boldsymbol{h}}_{\boldsymbol{x}} &= T_e^t r_e^{-1} \boldsymbol{H}_{\boldsymbol{x}} \\ \tilde{\boldsymbol{h}}_{\boldsymbol{z}} &= T_h^t r_h^{-1} \boldsymbol{H}_{\boldsymbol{z}}.\end{aligned} \tag{36}$$

Substituting our finite difference operators, the above relations and the transformations defined by (30) into equations (11)—(14) yields the following matrix relationship between the transformed tangential fields, $\boldsymbol{\Phi}_{\boldsymbol{y}}^{\mathrm{TE,TM}}$ and $(\partial/\partial y)\boldsymbol{\Phi}_{\boldsymbol{y}}^{\mathrm{TE,TM}}$

$$\begin{bmatrix}\tilde{\boldsymbol{e}}_{\boldsymbol{z}} \\ \tilde{\boldsymbol{e}}_{\boldsymbol{x}} \\ \tilde{\boldsymbol{h}}_{\boldsymbol{x}} \\ \tilde{\boldsymbol{h}}_{\boldsymbol{z}}\end{bmatrix} = \begin{bmatrix} \frac{1}{j}Q_{11} & \frac{1}{\gamma}Q_{12} & 0 & 0 \\ \frac{1}{j\gamma}Q_{21} & 0 & 0 & 0 \\ 0 & 0 & 0 & \frac{1}{j\gamma}Q_{34} \\ 0 & 0 & \frac{1}{\gamma}Q_{43} & \frac{1}{j}Q_{44} \end{bmatrix} \begin{bmatrix} \boldsymbol{\Phi}_{\boldsymbol{y}}^{\mathrm{TM}} \\ \frac{\partial}{\partial y}\boldsymbol{\Phi}_{\boldsymbol{y}}^{\mathrm{TE}} \\ \frac{\partial}{\partial y}\boldsymbol{\Phi}_{\boldsymbol{y}}^{\mathrm{TM}} \\ \boldsymbol{\Phi}_{\boldsymbol{y}}^{\mathrm{TE}} \end{bmatrix} \tag{37}$$

where the submatrices Q_{ij} are given in the Appendix for all lateral wall combinations.

Equation (37) holds for any vertical position within a layer. We can eliminate $\boldsymbol{\Phi}_{\boldsymbol{y}}^{\mathrm{TE,TM}}$ and $(\partial/\partial y)\boldsymbol{\Phi}_{\boldsymbol{y}}^{\mathrm{TE,TM}}$ by combining equation (37), written at positions y_a and y_b, with equation (35). After some algebraic manipulations we obtain the following matrix relationships between the transformed tangential fields at the top and bottom of j

$$\begin{aligned}\begin{bmatrix}\tilde{\boldsymbol{e}}_{\boldsymbol{z}}|_{y_a} \\ \tilde{\boldsymbol{e}}_{\boldsymbol{z}}|_{y_b}\end{bmatrix} &= \gamma Q_{11} Q_{21}^{-1} \begin{bmatrix}\tilde{\boldsymbol{e}}_{\boldsymbol{x}}|_{y_a} \\ \tilde{\boldsymbol{e}}_{\boldsymbol{x}}|_{y_b}\end{bmatrix} \\ &\quad + jQ_{12}[\gamma_e] \begin{bmatrix} -[\tanh(\gamma_e d)]^{-1} & [\sinh(\gamma_e d)]^{-1} \\ -[\sinh(\gamma_e d)]^{-1} & [\tanh(\gamma_e d)]^{-1} \end{bmatrix} \\ &\quad \cdot Q_{34}^{-1} \begin{bmatrix}\tilde{\boldsymbol{h}}_{\boldsymbol{x}}|_{y_a} \\ \tilde{\boldsymbol{h}}_{\boldsymbol{x}}|_{y_b}\end{bmatrix}\end{aligned} \tag{38}$$

$$\begin{aligned}\begin{bmatrix}\tilde{\boldsymbol{h}}_{\boldsymbol{z}}|_{y_a} \\ \tilde{\boldsymbol{h}}_{\boldsymbol{z}}|_{y_b}\end{bmatrix} &= jQ_{43}[\gamma_h] \begin{bmatrix} -[\tanh(\gamma_h d)]^{-1} & [\sinh(\gamma_h d)]^{-1} \\ -[\sinh(\gamma_h d)]^{-1} & [\tanh(\gamma_h d)]^{-1} \end{bmatrix} \\ &\quad \cdot Q_{21}^{-1} \begin{bmatrix}\tilde{\boldsymbol{e}}_{\boldsymbol{x}}|_{y_a} \\ \tilde{\boldsymbol{e}}_{\boldsymbol{x}}|_{y_b}\end{bmatrix} + \gamma Q_{44} Q_{34}^{-1} \begin{bmatrix}\tilde{\boldsymbol{h}}_{\boldsymbol{x}}|_{y_a} \\ \tilde{\boldsymbol{h}}_{\boldsymbol{x}}|_{y_b}\end{bmatrix}.\end{aligned} \tag{39}$$

Equations (38) and (39) can be combined into either an admittance type matrix

$$\begin{bmatrix}\tilde{\boldsymbol{h}}_{\boldsymbol{a}} \\ \tilde{\boldsymbol{h}}_{\boldsymbol{b}}\end{bmatrix} = \begin{bmatrix} y_1 & -y_2 \\ y_2 & -y_1 \end{bmatrix} \begin{bmatrix}\tilde{\boldsymbol{e}}_{\boldsymbol{a}} \\ \tilde{\boldsymbol{e}}_{\boldsymbol{b}}\end{bmatrix} \tag{40}$$

or alternatively, an impedance type matrix

$$\begin{bmatrix}\tilde{\boldsymbol{e}}_{\boldsymbol{a}} \\ \tilde{\boldsymbol{e}}_{\boldsymbol{b}}\end{bmatrix} = \begin{bmatrix} z_1 & -z_2 \\ z_2 & -z_1 \end{bmatrix} \begin{bmatrix}\tilde{\boldsymbol{h}}_{\boldsymbol{a}} \\ \tilde{\boldsymbol{h}}_{\boldsymbol{b}}\end{bmatrix} \tag{41}$$

where we have coalesced the following subvectors

$$\tilde{\boldsymbol{h}}_{\boldsymbol{a,b}} = \begin{bmatrix}\tilde{\boldsymbol{h}}_{\boldsymbol{z}}|_{y_{a,b}} \\ \tilde{\boldsymbol{h}}_{\boldsymbol{x}}|_{y_{a,b}}\end{bmatrix}, \quad \tilde{\boldsymbol{e}}_{\boldsymbol{a,b}} = \begin{bmatrix}\tilde{\boldsymbol{e}}_{\boldsymbol{x}}|_{y_{a,b}} \\ \tilde{\boldsymbol{e}}_{\boldsymbol{z}}|_{y_{a,b}}\end{bmatrix} \tag{42}$$

and submatrices

$$y_1 = \begin{bmatrix} -y_{11} & y_{12} \\ y_{21} & -y_{22} \end{bmatrix}, \quad y_2 = \begin{bmatrix} -y_{13} & y_{14} \\ y_{23} & -y_{24} \end{bmatrix} \tag{43}$$

$$z_1 = \begin{bmatrix} -z_{11} & z_{12} \\ z_{21} & -z_{22} \end{bmatrix}, \quad z_2 = \begin{bmatrix} -z_{13} & z_{14} \\ z_{23} & -z_{24} \end{bmatrix}. \tag{44}$$

The elemental matrices y_{ij} and z_{ij} are given in the Appendix.

In order to formulate our indirect eigenvalue problem, we must derive relationships between $\tilde{\boldsymbol{h}}$ and $\tilde{\boldsymbol{e}}$ at an interface where the tangential fields will be near their maximum, which is usually near the centre of the structure, say, the interface above layer j and below layer $j+1$. We obtain these relationships by working our way from the top and bottom limits while imposing the continuity condition to the tansformed tangential fields at layer interfaces. Starting from the bottom limit and working our way up to the interface at y_b in layer j we obtain, using (40), the following admittance type relationship [9]

$$\tilde{\boldsymbol{h}}_{\boldsymbol{b}}^{(j)} = Y^{(j)} \tilde{\boldsymbol{e}}_{\boldsymbol{b}}^{(j)} \tag{45}$$

with $Y^{(j)}$ defined recursively

$$Y^{(j)} = y_2^{(j)}[y_1^{(j)} - Y^{(j-1)}]^{-1} y_2^{(j)} - y_1^{(j)} \tag{46}$$

and where the admittance of the first layer depends on whether the bottom limit is an electric or magnetic wall

$$Y^{(1)} = \begin{cases} -y_1^{(1)} & \text{bottom ew} \\ y_2^{(1)}[y_1^{(1)}]^{-1} y_2^{(1)} - y_1^{(1)} & \text{bottom mw} \end{cases} \tag{47}$$

Similarly, working our way down from the top limit, we obtain the following equations which hold at position y_a within layer $j+1$.

$$\tilde{\boldsymbol{h}}_{\boldsymbol{a}}^{(j+1)} = Y^{(j+1)} \tilde{\boldsymbol{e}}_{\boldsymbol{a}}^{(j+1)} \tag{48}$$

$$Y^{(j+1)} = y_1^{(j+1)} - y_2^{(j+1)}[Y^{(j+2)} + y_1^{(j+1)}]^{-1} y_2^{(j+1)} \tag{49}$$

$$Y^{(N)} = \begin{cases} y_1^{(N)} & \text{top ew} \\ y_1^{(N)} - y_2^{(N)}[y_1^{(N)}]^{-1} y_2^{(N)} & \text{top mw} \end{cases} \tag{50}$$

In the same way, using (41), we derive an impedance type relationship for the bottom part

$$\tilde{\boldsymbol{e}}_{\boldsymbol{b}}^{(j)} = Z^{(j)} \tilde{\boldsymbol{h}}_{\boldsymbol{b}}^{(j)} \tag{51}$$

$$Z^{(j)} = z_2^{(j)}[z_1^{(j)} - Z^{(j-1)}]^{-1} z_2^{(j)} - z_1^{(j)} \tag{52}$$

$$Z^{(1)} = \begin{cases} z_2^{(1)}[z_1^{(1)}]^{-1} z_2^{(1)} - z_1^{(1)} & \text{bottom ew} \\ -z_1^{(1)} & \text{bottom mw} \end{cases} \tag{53}$$

and for the top part

$$\tilde{\boldsymbol{e}}_{\boldsymbol{a}}^{(j+1)} = Z^{(j+1)} \tilde{\boldsymbol{h}}_{\boldsymbol{a}}^{(j+1)} \tag{54}$$

$$Z^{(j+1)} = z_1^{(j+1)} - z_2^{(j+1)}[Z^{(j+2)} + z_1^{(j+1)}]^{-1} z_2^{(j+1)} \tag{55}$$

$$Z^{(N)} = \begin{cases} z_1^{(N)} - z_2^{(N)}[z_1^{(N)}]^{-1} z_2^{(N)} & \text{top ew} \\ z_1^{(N)} & \text{top mw} \end{cases}. \tag{56}$$

TABLE I
SUGGESTED FORMULATION FOR THE MODAL MATRICES

T & B Walls	$\tilde{G}_e$	$\tilde{G}_h$
ew-ew	$Y^{(j+1)} - Y^{(j)}$	$[Y^{(j+1)}]^{-1} - [Y^j]^{-1}$
mw-ew	$[Z^{(j+1)}]^{-1} - Y^j$	$Z^{(j+1)} - [Y^{(j)}]^{-1}$
mw-mw	$[Z^{(j+1)}]^{-1} - [Z^{(j)}]^{-1}$	$Z^{(j+1)} - Z^{(j)}$
ew-mw	$Y^{(j+1)} - [Z^{(j)}]^{-1}$	$[Y^{(j+1)}]^{-1} - Z^{(j)}$

We now define our indirect eigenvalue problem by applying the field matching condition one last time at the interface between layers j and $j+1$, yielding a modal matrix for the transformed tangential electric fields

$$\tilde{G}_e(\gamma)\tilde{\boldsymbol{e}}_{\boldsymbol{b}}^{(j)} = 0 \tag{57}$$

or alternatively for the transformed tangential magnetic fields

$$\tilde{G}_h(\gamma)\tilde{\boldsymbol{h}}_{\boldsymbol{b}}^{(j)} = 0. \tag{58}$$

Either of the above modal functions will generate solutions for γ by making the determinant null

$$\det[\tilde{G}_{e,h}(\gamma)] = 0. \tag{59}$$

We may construct the modal matrices $\tilde{G}_{e,h}$ by combining the admittance and impedance matrices (45), (48), (51) and (54) in many ways that are, theoretically, equivalent. However, from a numerical standpoint some combinations may prove to be more efficient and stable. For example, if the bottom limit is a magnetic wall, then the construction of the impedance matrix $Z^{(1)}$, from (53), requires fewer operations than the construction of the admittance matrix $Y^{(1)}$, from (47); of course the opposite is true if an electric wall defines the bottom limit. Furthermore, we note from the Appendix, that the submatrices comprising z_1 and y_1 contain tanh functions, $[\gamma_{e,h}]$ matrices, Q_{ij} submatrices and constants suggesting that z_1 and y_1 may be numerically stable regardless of layer thicknesses. This is not true of matrices z_2 and y_2 as the functions sinh become problematic for large arguments, therefore, for thick layers. It is thus preferable to select combinations of the admittance and impedance matrices in such a way that the first and last layers are modeled using only z_1 or y_1 matrices depending on the limits. This capability is quite useful when analysing waveguides that exhibit quarter structure symmetry as bottom magnetic walls are often used to generate a specific family of modes. From these arguments, we gather that the modal functions $\tilde{G}_{e,h}$ are best constructed according to the equations in Table I, given for all possible combinations of top and bottom walls.

The flexibility gained, by being able to efficiently construct both modal matrices G_e or G_h, is interesting when solving equation (59) since certain modes may be easier to find with one matrix compared to the other. This is due to the fact that the matrices are constructed on the basis of matching tangential electric or magnetic fields which vary in strength relative to each other, depending on the desired mode.

III. NUMERICAL RESULTS AND DISCUSSION

In this section, modal dispersion curves are given for a series of lossy and lossless anisotropic inhomogeneous waveguides useful at millimeter-wave or optical frequencies. Results obtained using the formulation given in the previous section, are compared with results available from the literature. We have adopted the modal identification convention found in [16] for all guides analyzed.

A. Lossy Anisotropic Image Waveguide

The shielded lossy anisotropic image waveguide, shown in the inset of Fig. 3, was analyzed. The dispersion curves of the E_y^{11} and E_y^{21} modes, propagating in this structure are given as a function of normalized frequency. As can be seen from the graphs, results reported in [3] for the E_y^{11} mode are in excellent agreement with ours.

The dispersion curves of the E_y^{11} mode were generated by placing a vertical magnetic wall through the centre and analysing half the structure; the curves for the E_y^{21} mode were obtained by applying electric wall symmetry. In both cases the dielectric discontinuity was placed on an E line and equations (26) and (27) applied. All calculations were performed by an HP9000 model 715/100 workstation. About two CPU minutes are required to obtain the root of equation (59) to a relative accuracy of 10^{-12}. Less than two megabytes of memory were required to model half the structure with 52 E and H lines.

To thoroughly validate our formulation we analyzed the structure obtained by taking the dual of the original one, with the modes of interest now being the H_y^{11} and H_y^{21} modes. As expected, the propagation constants we obtained are identical to those found for the original image guide. All cases were verified with μ'_{yy} succesively taking on the values: 1.0, 1.5 and 2.0. The discontinuity in permeability was placed on an H line and (28) and (29) applied.

B. Anisotropic Dielectric Waveguide

The open dielectric structure shown in the inset of Fig. 4 has been analyzed and the results plotted as a function of normalized frequency. As can be seen, the dispersion curves that we have obtained for the first four modes agree quite well with those given in [3]. We have analyzed a quarter of the structure using appropriate vertical and horizontal symmetry walls placed in the centre of the guide to generate the desired modes. The computation domain was bounded with electric or magnetic walls which were placed, using a nonequidistant discretization, far enough from the guide to have no calculable effects on the results. Specifically, the lateral and top walls were placed at distances of about $10a$ and $10b$ respectively, where a and b are the dimensions of the guide.

It is well known that the first two modes of an open dielectric waveguide, E_x^{11} and E_y^{11}, do not have cut-off frequencies if the structure exhibits both horizontal and vertical symmetry with respect to its center. At low frequencies, these modes become particularly sensitive to boundary conditions that are not placed far enough from the guide, especially if the latter is weakly guiding such as the structure modeled here. Absorbing boundary conditions or the ability to place normal boundary

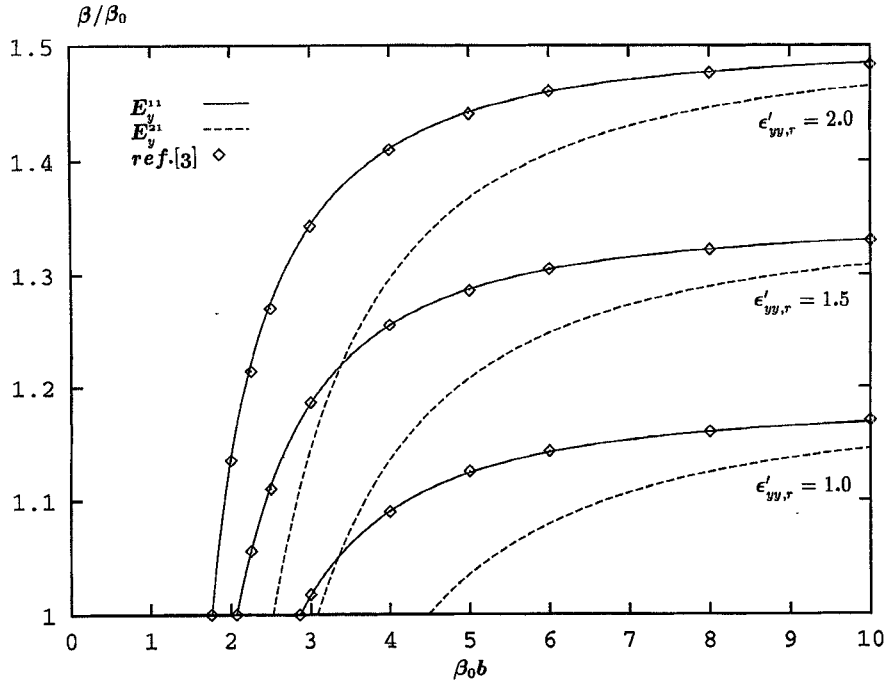

(a)

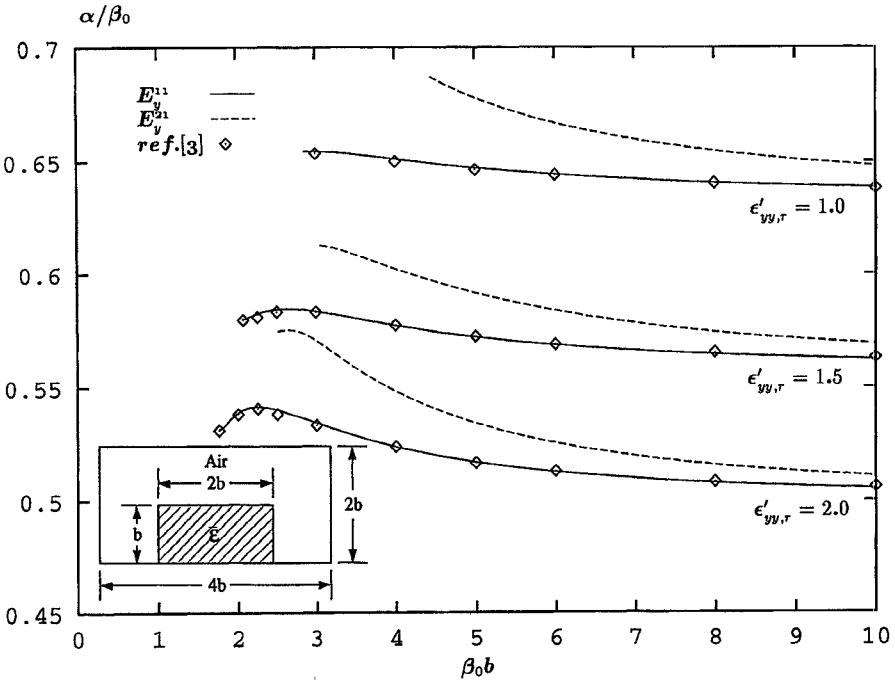

(b)

Fig. 3. Dispersion characteristics of the E_y^{11} and E_y^{21} modes propagating in a shielded lossy anisotropic image guide. (a) Normalized phase constant. (b) Normalized attenuation constant. The relative permeabilities of the dielectric are: $\epsilon_{xx,r} = \epsilon_{zz,r} = 1.5 - j1.5$ and $\epsilon_{yy,r} = \epsilon'_{yy,r} - j1.5$, where $\epsilon'_{yy,r} = 1.0, 1.5$ or 2.0.

conditions far from the guide are essential if we are to obtain dispersion curves that come down asymptotically toward the abscissa with decreasing frequency, as shown in Fig. 4.

C. $LiNbO_3$ *Optical Waveguide*

The $LiNbO_3$ channel optical waveguide shown in the inset of Fig. 5 has been analyzed. The dispersion curves of the first four modes were computed by exploiting the vertical symmetry of the structure about its center. The calculation domain was bounded by lateral, top and bottom walls placed at distances of 45 μm, 10 μm, and 24 μm, respectively, from the guide. A nonequidistant discretization scheme was used. We have compared our results to those reported in [1]; as shown in Fig. 5, agreement is good.

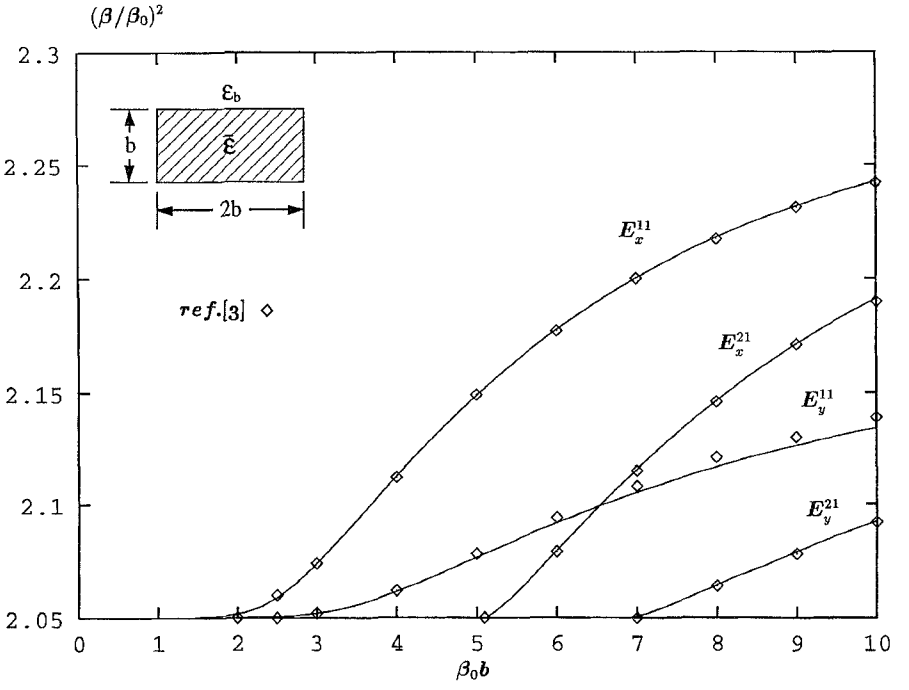

Fig. 4. Normalized dispersion characteristics of the first four modes propagating in a lossless open anisotropic dielectric waveguide. The relative permeabilities of the guide are: $\epsilon_{xx,r} = \epsilon_{zz,r} = 2.31, \epsilon_{yy,r} = 2.19$, and the background: $\epsilon_{b,r} = 2.05$.

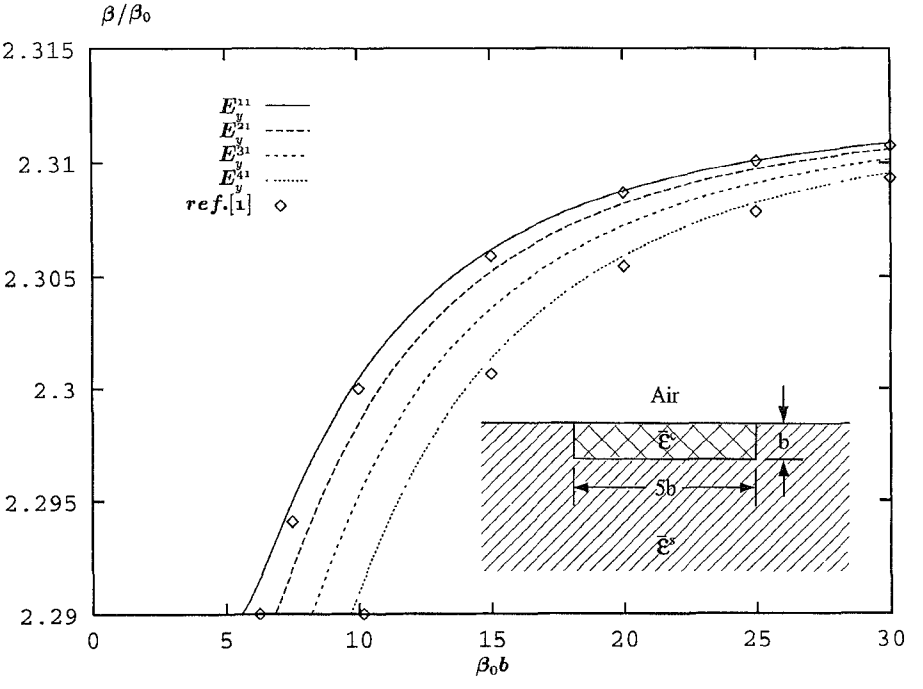

Fig. 5. Normalized dispersion characteristics of the first four modes propagating in a $LiNbO_3$ optical waveguide having the following relative permeabilities in the channel: $\epsilon^c_{xx,r} = (2.22)^2, \epsilon^c_{yy,r} = \epsilon^c_{zz,r} = (2.3129)^2$ and in the substrate: $\epsilon^s_{xx,r} = (2.2)^2, \epsilon^s_{yy,r} = \epsilon^s_{zz,r} = (2.29)^2$. In this case, $b = 1.0\ \mu$m.

D. Effect of Anisotropy in Dielectric Waveguides

As a final example, we have modeled the structure shown in the inset of Fig. 6 using various tensors $\bar{\epsilon}$ and $\bar{\mu}$ in the guide while maintaining the background permittivity and permeability constant to values of $\epsilon_{b,r} = 2.0$ and $\mu_{b,r} = 1.0$. The dispersion curves for the E_x^{11} and E_y^{11} modes have been computed for the case study described in Table II and are given in Fig. 6. We have limited our study to these two modes since they are the first members of the E_x^{mn} and E_y^{mn} families and are polarized mainly along the x and y axes, respectively.

The guide described by case 1 is isotropic and forms the basis of our comparisons. We note in this case that the E_x^{11}

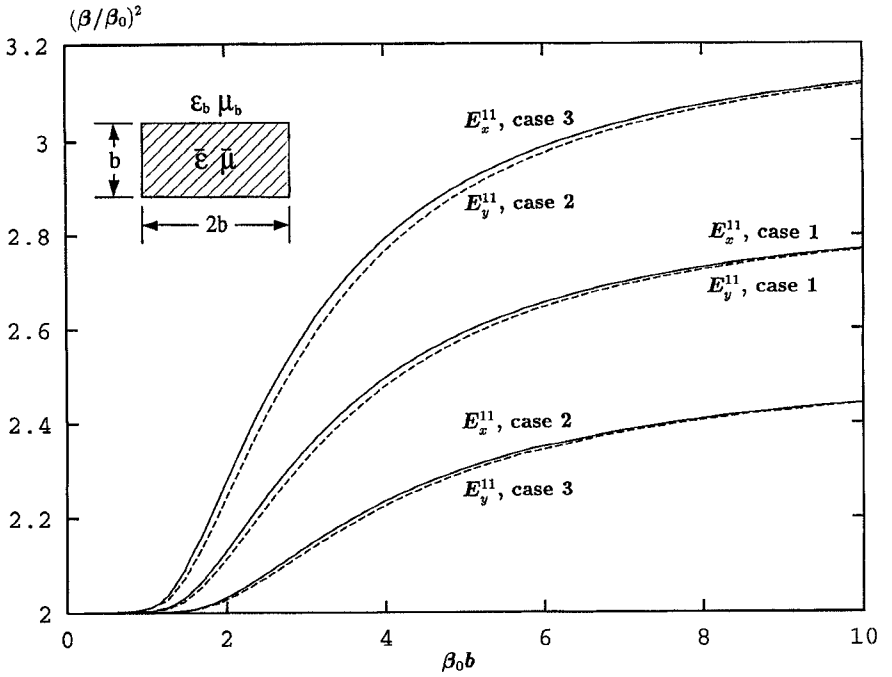

Fig. 6. Normalized dispersion characteristics of the E_x^{11} and E_y^{11} modes in an open dielectric waveguide as a function of anisotropy; the case study is described in Table II.

TABLE II
DESCRIPTION OF THE CASE STUDY FOR THE STRUCTURE SHOWN IN THE INSET OF FIG. 6

	Case 1	Case 2	Case 3
$\bar{\epsilon}_r$	$\epsilon_{xx,r} = 2.6$	$\epsilon_{xx,r} = 2.4$	$\epsilon_{xx,r} = 2.8$
	$\epsilon_{yy,r} = 2.6$	$\epsilon_{yy,r} = 2.8$	$\epsilon_{yy,r} = 2.4$
	$\epsilon_{zz,r} = 2.6$	$\epsilon_{zz,r} = 2.6$	$\epsilon_{zz,r} = 2.6$
$\bar{\mu}_r$	$\mu_{xx,r} = 1.10$	$\mu_{xx,r} = 1.15$	$\mu_{xx,r} = 1.05$
	$\mu_{yy,r} = 1.10$	$\mu_{yy,r} = 1.05$	$\mu_{yy,r} = 1.15$
	$\mu_{zz,r} = 1.10$	$\mu_{zz,r} = 1.10$	$\mu_{zz,r} = 1.10$

and E_y^{11} modes are characterized by dispersion curves that are very close together; these modes would be degenerate if the aspect ratio was unitary. Making the horizontal dimension larger than the vertical favors the E_x^{11} mode in the sense that it makes its propagation constant larger than that of the E_y^{11} mode for a given frequency.

The tensors given as case 2 have been selected to favor the E_y^{11} mode at the expense of the E_x^{11} mode. As shown by the dispersion curves, E_y^{11} is now characterized by propagation constants that are much larger than those of E_x^{11}. Furthermore, both curves are located far above and below the curves belonging to the isotropic guide. In case 3, our tensors have been reoriented to favor the E_x^{11} mode at the expense of the E_y^{11} mode. As expected, the propagation constants of E_x^{11} are now much larger than those belonging to E_y^{11}.

It is interesting to note that the dispersion curve of the E_x^{11} mode in case 3 is slightly above the curve of the E_y^{11} mode in case 2. The same behavior is noted when comparing the E_x^{11} mode of case 2 with the E_y^{11} mode of case 3. These observations are consistent with the geometrical effects engendered by a nonunity aspect ratio dielectric guide, as outlined above.

Based on the results presented in this case study and supported by those reported in [4], we see that the orientation of the tensors comprising the dielectric guide has the important effect of seperating the dispersion curves of the first vertically and horizontally polarized modes E_x^{11} and E_y^{11} favoring one at the expense of the other. This implies that in a low aspect ratio asymmetric guide, where the E_x^{11} and E_y^{11} modes have nonzero cut-off frequencies, wideband monomode operation could be obtained for either polarization, depending on the orientation of tensors.

IV. CONCLUSION

A formulation based on the method of lines has been presented to model a class of waveguide structures constructed from lossy inhomogeneous anisotropic materials characterized by complex diagonalized permittivity and permeability tensors. The validity of our approach has been demonstrated for both millimeter-wave and optical guides. Alternate modal matrices have been derived in order to increase the numerical stability, efficiency and accuracy of the method when using magnetic walls as top and bottom boundary conditions. The flexibility gained by introducing these modal matrices also aids in finding the roots of the determinant equation.

APPENDIX

A. Submatrices Q_{ij}

The submatrices Q_{ij} defined by (37) are given below for an inhomogeneous layer. The top notation is related to ew-ew or ew-mw lateral boundary conditions while the bottom refers

to mw-mw or mw-ew conditions

$$Q_{11} = \begin{cases} -\dfrac{1}{\omega h} T_e^t [\epsilon_{zz}]_e^{-1} D_x^t U_h \\ \dfrac{1}{\omega h} T_e^t [\epsilon_{zz}]_e^{-1} D_x U_h \end{cases}$$

$$Q_{12} = T_e^t [\epsilon_{yy}]_e [\epsilon_{zz}]_e^{-1} U_e$$

$$Q_{21} = \begin{cases} \dfrac{1}{\omega h^2} T_h^t D_x [\epsilon_{zz}]_e^{-1} D_x^t U_h - \omega T_h^t [\mu_{yy}]_h U_h \\ \dfrac{1}{\omega h^2} T_h^t D_x^t [\epsilon_{zz}]_e^{-1} D_x U_h - \omega T_h^t [\mu_{yy}]_h U_h \end{cases}$$

$$Q_{34} = \begin{cases} -\dfrac{1}{\omega h^2} T_e^t D_x^t [\mu_{zz}]_h^{-1} D_x U_e + \omega T_e^t [\epsilon_{yy}]_e U_e \\ -\dfrac{1}{\omega h^2} T_e^t D_x [\mu_{zz}]_h^{-1} D_x^t U_e + \omega T_e^t [\epsilon_{yy}]_e U_e \end{cases}$$

$$Q_{43} = T_h^t [\mu_{yy}]_h [\mu_{zz}]_h^{-1} U_h$$

$$Q_{44} = \begin{cases} -\dfrac{1}{\omega h} T_h^t [\mu_{zz}]_h^{-1} D_x U_e \\ \dfrac{1}{\omega h} T_h^t [\mu_{zz}]_h^{-1} D_x^t U_e. \end{cases}$$

The following inversions are obtained analytically:

$$Q_{12}^{-1} = U_e^{-1} [\epsilon_{zz}]_e [\epsilon_{yy}]_e^{-1} T_e$$
$$Q_{43}^{-1} = U_h^{-1} [\mu_{zz}]_h [\mu_{yy}]_h^{-1} T_h.$$

For a homogeneous layer, the submatrices Q_{ij} are simplified

$$Q_{11} = \begin{cases} -\dfrac{1}{\omega h \epsilon_{zz}} T_e^t D_x^t T_h = -\dfrac{1}{\omega h \epsilon_{zz}} \delta^t \\ \dfrac{1}{\omega h \epsilon_{zz}} T_e^t D_x T_h = \dfrac{1}{\omega h \epsilon_{zz}} \delta \end{cases}$$

$$Q_{12} = \frac{\epsilon_{yy}}{\epsilon_{zz}} I$$

$$Q_{21} = \frac{1}{\omega h^2 \epsilon_{zz}} [\lambda_h^2] - \omega \mu_{yy} I$$

$$Q_{34} = -\frac{1}{\omega h^2 \mu_{zz}} [\lambda_e^2] + \omega \epsilon_{yy} I$$

$$Q_{43} = \frac{\mu_{yy}}{\mu_{zz}} I$$

$$Q_{44} = \begin{cases} -\dfrac{1}{\omega h \mu_{zz}} T_h^t D_x T_e = -\dfrac{1}{\omega h \mu_{zz}} \delta \\ \dfrac{1}{\omega h \mu_{zz}} T_h^t D_x^t T_e = \dfrac{1}{\omega h \mu_{zz}} \delta^t \end{cases}$$

where the matrix δ is as given in [7] and I represents the identity matrix.

B. Submatrices y_{ij} and z_{ij}

The submatrices y_{ij} are written

$$y_{11} = \jmath Q_{43} [\gamma_h] [\tanh(\gamma_h d)]^{-1} Q_{21}^{-1} + \jmath \gamma^2 Q_{44} [\tanh(\gamma_e d)]^{-1} [\gamma_e]^{-1} Q_{12}^{-1} Q_{11} Q_{21}^{-1}$$

$$y_{12} = \jmath \gamma Q_{44} [\tanh(\gamma_e d)]^{-1} [\gamma_e]^{-1} Q_{12}^{-1}$$

$$y_{13} = \jmath Q_{43} [\gamma_h] [\sinh(\gamma_h d)]^{-1} Q_{21}^{-1} + \jmath \gamma^2 Q_{44} [\sinh(\gamma_e d)]^{-1} [\gamma_e]^{-1} Q_{12}^{-1} Q_{11} Q_{21}^{-1}$$

$$y_{14} = \jmath \gamma Q_{44} [\sinh(\gamma_e d)]^{-1} [\gamma_e]^{-1} Q_{12}^{-1}$$

$$y_{21} = \frac{\gamma}{\jmath} Q_{34} [\tanh(\gamma_e d)]^{-1} [\gamma_e]^{-1} Q_{12}^{-1} Q_{11} Q_{21}^{-1}$$

$$y_{22} = \frac{1}{\jmath} Q_{34} [\tanh(\gamma_e d)]^{-1} [\gamma_e]^{-1} Q_{12}^{-1}$$

$$y_{23} = \frac{\gamma}{\jmath} Q_{34} [\sinh(\gamma_e d)]^{-1} [\gamma_e]^{-1} Q_{12}^{-1} Q_{11} Q_{21}^{-1}$$

$$y_{24} = \frac{1}{\jmath} Q_{34} [\sinh(\gamma_e d)]^{-1} [\gamma_e]^{-1} Q_{12}^{-1}$$

and the submatrices z_{ij}

$$z_{11} = \frac{1}{\jmath} Q_{21} [\tanh(\gamma_h d)]^{-1} [\gamma_h]^{-1} Q_{43}^{-1}$$

$$z_{12} = \frac{\gamma}{\jmath} Q_{21} [\tanh(\gamma_h d)]^{-1} [\gamma_h]^{-1} Q_{43}^{-1} Q_{44} Q_{34}^{-1}$$

$$z_{13} = \frac{1}{\jmath} Q_{21} [\sinh(\gamma_h d)]^{-1} [\gamma_h]^{-1} Q_{43}^{-1}$$

$$z_{14} = \frac{\gamma}{\jmath} Q_{21} [\sinh(\gamma_h d)]^{-1} [\gamma_h]^{-1} Q_{43}^{-1} Q_{44} Q_{34}^{-1}$$

$$z_{21} = \jmath \gamma Q_{11} [\tanh(\gamma_h d)]^{-1} [\gamma_h]^{-1} Q_{43}^{-1}$$

$$z_{22} = \jmath Q_{12} [\gamma_e] [\tanh(\gamma_e d)]^{-1} Q_{34}^{-1} + \jmath \gamma^2 Q_{11} [\tanh(\gamma_h d)]^{-1} [\gamma_h]^{-1} Q_{43}^{-1} Q_{44} Q_{34}^{-1}$$

$$z_{23} = \jmath \gamma Q_{11} [\sinh(\gamma_h d)]^{-1} [\gamma_h]^{-1} Q_{43}^{-1}$$

$$z_{24} = \jmath Q_{12} [\gamma_e] [\sinh(\gamma_e d)]^{-1} Q_{34}^{-1} + \jmath \gamma^2 Q_{11} [\sinh(\gamma_h d)]^{-1} [\gamma_h]^{-1} Q_{43}^{-1} Q_{44} Q_{34}^{-1}$$

where d refers to the thickness of the current layer, where matrices Q_{ij} and $[\gamma_{e,h}]$ are known.

REFERENCES

[1] B. M. A. Rahman and J. B. Davies, "Finite-element solution of integrated optical waveguides," *IEEE/OSA J. Lightwave Technol.*, vol. LT-2, pp. 682–688, Oct. 1984.

[2] K. Hayata, K. Miura, and M. Koshiba, "Finite-element formulation for lossy waveguides" *IEEE Trans. Microwave Theory Tech.*, vol. 36, pp. 268–276, Feb. 1988.

[3] Y. Lu and F. A. Fernandez, "An efficient finite element solution of inhomogeneous anisotropic and lossy dielectric waveguides," *IEEE Trans. Microwave Theory Tech.*, vol. 41, pp. 1215–1223, June/July 1993.

[4] C. L. da Silva Souza Sobrinho and A. J. Giarola, "Analysis of biaxially anisotropic dielectric waveguides with Gaussian-Gaussian index of refraction profiles by the finite-difference method," *IEE Proc., part H*, vol. 140, pp. 224–230, June 1993.

[5] H. Diestel, "A method for calculating inhomogeneous planar dielectric waveguides (in German)," Ph.D. dissertation, Fern Univ., Hagen, Germany, 1984.

[6] ——, "A method for calculating the guided modes of strip-loaded optical waveguides with arbitrary index profile". *IEEE J. Quantum Electron.*, vol. QE-20, pp. 1288–1293, Nov. 1984.

[7] R. Pregla and W. Pascher "The method of lines," in *Numerical Techniques for Microwave and Millimeter-Wave Passive Structures* T. Itoh, Ed. New York: Wiley, 1989.

[8] U. Rogge and R. Pregla, "Method of lines for the analysis of strip-loaded optical waveguides," *J. Opt. Soc. Am., part B*, vol. 8, pp. 459–463, Feb. 1991.

[9] ——, "Method of lines for the analysis of dielectric waveguides," *IEEE/OSA J. Lightwave Technol.y*, vol. 11, pp. 2015–2020, Dec. 1993.

[10] F. J. Schmückle and R. Pregla, "The method of lines for the analysis of lossy planar waveguides," *IEEE Trans. Microwave Theory Tech.*, vol. 38, pp. 1473–1479, Oct. 1990.

[11] K. Wu, R. Vahldieck, J. L. Fikart, and H. Minkus, "The influence of finite conductor thickness and conductivity on fundamental and higher-order modes in miniature hybrid MIC's (MHMIC's) and MMIC's," *IEEE Trans. Microwave Theory Tech.*, vol. 41, pp. 421–430, Mar. 1993.

[12] B. M. Sherrill and N. G. Alexópoulos, "The method of lines applied to a finline/strip configuration on an anisotropic substrate," *IEEE Trans. Microwave Theory Tech.*, vol. 35, pp. 568–574, June 1987.

[13] J. Gerdes, K. H. Helf, and R. Pregla "Full-wave analysis of traveling-wave electrodes with finite thickness for electro-optic modulators by the method of lines," *IEEE/OSA J. Lightwave Technol.*, vol. 9, pp. 461–467, Apr. 1991.

[14] R. Pregla, "Method of lines for the analysis of multilayered gyrotropic waveguide structures," *IEE Proc., part H*, vol. 140, pp. 183–192, June 1993.
[15] H. Diestel and S. B. Worm, "Analysis of hybrid field problems by the method of lines with nonequidistant discretization," *IEEE Trans. Microwave Theory Tech.*, vol. 32, pp. 633–638, June 1984.
[16] J. E. Goell, "A circular-harmonic computer analysis of rectangular dielectric waveguides," *Bell Syst. Tech. J.*, pages pp. 2133–2160, Sept. 1969.

Pierre Berini (SM'93–M'96) was born in 1966, in Timmins, Ontario, Canada. He received the B.Sc. degree in computer science and the B.E.Sc. degree in electrical engineering both in 1990 from the University of Western Ontario, London, Canada. He received the M.Sc.A. and Ph.D. degrees in electrical engineering in 1992 and 1995, respectively, from l'École Polytechnique de Montréal, Montréal, Canada.

He joined the Department of Electrical Engineering at the University of Ottawa in January 1996 where he is now an Assistant Professor. His main research interests include the numerical modeling of electromagnetic fields for optoelectronic, millimeterwave and microwave applications. He also has interests in the design and characterization of passive structures and active (non)linear microwave circuits.

Ke Wu (M'87–SM'92) was born in Jiangsu, China. He received the B.Sc. degree (with distinction) in radio engineering from the Nanjing Institute of Technology (now Southeast University), Nanjing, China, and the D.E.A. degree in electronics and Ph.D. degree (with distinction) in optics, optoelectronics, and microwave engineering from the Institut National Polytechnique de Grenoble (INPG), France.

From 1983 to 1987, he conducted research in the Laboratoire d'\'Electromagnetisme, Microondes et Opto-électronique (LEMO), Grenoble, France. From 1988 to 1992 he was a Research Associate at the University of Victoria, Victoria, B.C., Canada. In 1992, he joined the Département de génie électrique et de génie informatique at the École Polytechnique de Montréal where he is now an Associate Professor. His main research interests include the analysis and design of various microwave/millimeter-wave integrated circuits and antennas, high-speed interconnects and packaging effects, numerical methods, dielectric material characterization, and superconducting devices. He is also interested in research and design of broadband optoelectronic components and lightwave transmission systems with emphasis on traveling-wave electro-optic modulators, couplers and switches.

Dr. Wu received a U.R.S.I. Young Scientist Award, and the Oliver Lodge Premium from the IEE. He serves on the editorial or review board of various technical journals and he provides consulting services to a number of industries and government agencies.